2008 IEEE International Conference on
Robotics and Automation
Pasadena, CA, USA, May 19-23, 2008

Swimming Capsule Endoscope using static and RF magnetic field of MRI for propulsion

Gábor Kósa, Péter Jakab, Ferenc Jólesz and Nobuhiko Hata, *Member, IEEE*

***Abstract*—Capsule endoscopy is a promising technique for diagnosing diseases in the small intestines. Here we propose a miniature swimming mechanism that uses MRI's magnetic fields for both propulsion and wireless energy delivery. Our method uses both the static and radio frequency (RF) magnetic field inherently available in MRI to generate propulsion force. The propulsion force is produced by a swimming tail containing waving beam consisting of three coils in a row. Alternating current in the coils acting on the static magnetic field of the MRI will generate waving movement to produce a propulsion force. RF magnetic field will provide power to generate the alternating currents in the coils. We developed a theoretical model to predict sinusoidal waves produced by the waving beam using the Euler-Bernoulli beam equation and multiple-input multiple-output system were solved using antenna design theory. This numerical model predicted that the maximal propulsion from a 10 mm long tail can produce a velocity of 7.9 mm/s force of 5.5 mN when placed in a 3T static magnetic field. A validation study with a single coil demonstrated that the theoretical and numerical model predicts well the proposed swimming mechanism and it is useful for the fabrication of swimming tails.**

I. Introduction

THE capsule endoscope has been the focus of discussion in the diagnosis of small intestine bleeding and the detection of Crohn's Disease, celiac disease and other malabsorption disorders, as well as benign and malignant tumors of the small intestine [1]. The capsule endoscope can reach areas of the small intestine that a conventional endoscope cannot [2]. More than one million procedures to examine the small intestine are performed annually in the United States. To aide in these procedures, the capsule endoscope has shown promise to become a first-line tool for diagnosis.

Although the capsule endoscopy is better than other available techniques at detecting sources of small bowel bleeding, it does not achieve 100% detection. The capsule is purely diagnostic and cannot be used to take biopsies, apply therapy, or mark abnormalities for surgery. Moreover, the position of capsule cannot be controlled. Once within the area of interest and a suspicious abnormality, it's movement cannot be controlled to better visualize the suspicious lesion.

Active steering of the capsule endoscope is a solution to this rather significant problem, and efforts are underway to make this functionality possible. Ishiyama and colleagues proposed the use of a magnetic field in driving the capsule endoscope [3]. They have shown that a magnetic actuator composed of a magnet and spiral tail can be steered wirelessly. By applying an external rotational magnetic field, the actuator was rotated and propelled wirelessly. They demonstrated that the actuator with 1-mm height spiral could move at 5 mm/s. Stefanini and colleagues proposed miniature legs to drive the capsule in the GI tract using electromagnetic induction as the energy supply [4], [5].

Here we propose the use of a miniature swimming mechanism relying on the MRI's magnetic field for both propulsion and for wireless energy delivery. Our method uses the static and the radio frequency (RF) magnetic field, namely the B0 and B1 magnetic field, inherently available in the MRI to generate the propulsion force. The device includes three tails with three coils in each. The RF magnetic field of the MRI supplies power for the electric current generation. Use of the MRI is further recommended to localize the swimming-robot in cross-sectional images. This localization ability will help the operator to maneuver the capsule toward the target organ more quickly and thereby reduce the overall examination time. Specifically, this paper reports on the theoretical design of the swimming mechanism and on an experimental study that was conducted to assess the validity of this theory.

II. Swimming in the MRI

A. Goal

Our goal was to develop and evaluate a swimming mechanism inspired by the flagellar movement of microorganisms. The mechanism was to produce a force of about 5 mN through three waving tails (Fig. 1). This strength was chosen based on literature of other swimming endoscope [4][5]. We designed an optimal waveform to drive the tails. The tails may propel the capsule to achieve a forward speed of about 5 mm/sec without load and about 2 mm/s with a standard capsule endoscope [1]. The size of the micro robot will be 10 mm in diameter and 20 mm long including the

Manuscript received September 14, 2007.

G. Kósa is with the Computer Vision Laboratory at ETH, Zurich, 8092 Switzerland (phone: +41 44 6327689; fax: +41 44 6321199; e-mail: gkosa@vision.ee.ethz.ch).

P. Jakab, F. Jólesz and N. Hata are with the Division of MRI and Image Guided Therapy Program at Department of Radiology, Brigham and Women's Hospital, Boston, MA and Harvard Medical School, Boston, MA 02115 USA (e-mail: {Jakab, Hata, Jolesz}@bwh.harvard.edu).

three swimming tails.

B. Propulsive principle

The swimming action in the micro world is different from

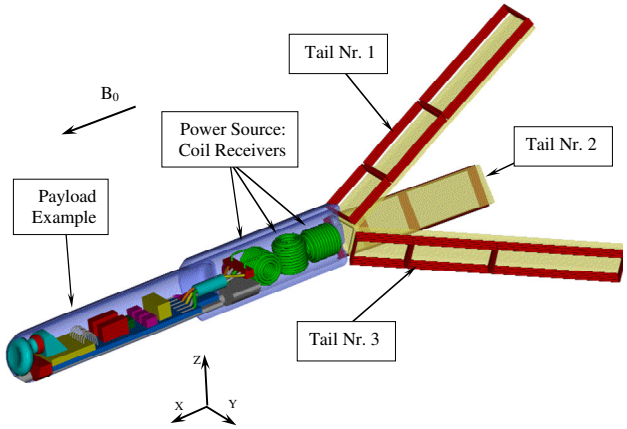

Fig. 1. Steerable swimming micro robot for the MRI.

the macro world. The hydrodynamic equations are scaled to the size of the swimmers. The low Reynolds number (Re<1) in micro flow enables omitting the inertial terms from the Navier-Stokes equation and confines them to the viscous flow environment where the Stokes equation is dominant [6].

In addition, in viscous flow the linearity of the Stokes equation prohibits the use of repeated motion such like a fish tail to generate propulsion force [7]. Swimming in viscous flow may be achieved through undulatory action alone. Taylor was the first to solve this fluidic problem for micro-mechanism to swim in viscous fluid to generate propulsion force [8].

Following Taylor's theoretical basis [8] and inspired by the flagellar movement of microorganisms, we found that the oscillating beam can create approximated sinusoidal traveling wave in viscous flow and to produce propulsion force effectively [9]-[11]. The sinusoidal wave from such tail can be decomposed as,

$$\begin{aligned} w^{(d)}(x,t) &= w\sin\kappa(x-Ut) = \\ &= w(\sin\kappa x\cos\kappa Ut - \cos\kappa x\sin\kappa Ut) = \\ &= \sum_{k=1}^{\infty}(Cs_k\cos\kappa Ut - Cc_k\sin\kappa Ut)\phi_k(x) = \\ &= \sum_{k=1}^{\infty} g_k^{(d)}(t)\phi_k(x) \approx \sum_{k=1}^{3} G_k\sin(\Omega t-\Phi_k)\phi_k(x) \end{aligned} \quad (1)$$

where w, κ and U are the amplitude, wave number and wave velocity accordingly of the desired advancing wave $w^{(d)}(x,t)$ in the beam. Cs_k and Cs_k are the decomposition of functions $\sin\kappa x$ and $\cos\kappa x$ into the modal functions, $\phi_k(x)$, of the k-th mode of the beam. $g_k^{(d)}(t)$ is the desired time function of the k-th mode that has to be created in the beam in order to achieve the desired traveling wave $w^{(d)}(x,t)$.

The number of coils in a tail is equal to the number of time functions $g_k^{(d)}(t)$, we can control. At least two coils are needed to create undulatory motion in the tail. Using a large number of coils increases the driving frequency and also creates technological difficulties. Therefore we chose to use three coils in the swimming tails. To create the phases Φ_k and amplitudes G_k in (1) one has to take into consideration the beam's dynamical response.

Extending this preliminary work of a single oscillating beam, we propose three elongated tails, each having three adjacent coils in a row (Fig. 1). We assume that there is no interaction between the fluidic motion created by each tail.

C. A swimming actuator in the MRI

Our goal here is to find the input currents that will create the amplitudes $\{G_1, G_2, G_3\}$ and the phases $\{\Phi_1, \Phi_2, \Phi_3\}$ in equation (1) which cause the beam to vibrate in a sinusoidal traveling wave. This problem is similar to an inverse kinematics problem of a robot.

Tail's vibration can be divided into three segments. $w_1(x,t)$ is the lateral motion of the tail in the area bounded by coil number one closest to the head unit, defined by $x=[0,\alpha_1 L]$. Similarly $w_2(x,t)$ is the lateral motion at the middle coil, $x=[\alpha_1 L,\alpha_2 L]$, and $w_3(x,t)$ is the lateral motion at the last coil therein the end of the tail, $x=[\alpha_2 L, L]$. Fig. 2 shows the distribution of the moments and forces along the swimming tail.

The motion of the tail is governed by the Euler-Bernoulli beam equations

$$\begin{aligned} m_1\frac{\partial^2 w_1(x,t)}{\partial t^2} + c\frac{\partial w_1(x,t)}{\partial t} + \hat{\mathcal{K}}_1\frac{\partial^4 w_1(x,t)}{\partial x^4} &= 0 \forall x=[0,\alpha_1 L] \\ m_2\frac{\partial^2 w_2(x,t)}{\partial t^2} + c\frac{\partial w_1(x,t)}{\partial t} + \hat{\mathcal{K}}_2\frac{\partial^4 w_2(x,t)}{\partial x^4} &= 0 \forall x=[\alpha_1 L,\alpha_2 L] \\ m_3\frac{\partial^2 w_3(x,t)}{\partial t^2} + c\frac{\partial w_1(x,t)}{\partial t} + \hat{\mathcal{K}}_3\frac{\partial^4 w_3(x,t)}{\partial x^4} &= 0 \forall x=[\alpha_1 L, L] \end{aligned} \quad (2)$$

where m_i is the distributed mass of each segment, c is the damping coefficient and $\hat{\mathcal{K}}_i$ is the elastic stiffness of each segment. The parameters above are not detailed due to space limitations, for further details see [9]-[11].

The boundary conditions for the beam are

$$\begin{aligned} @\, x=0 \qquad\qquad\qquad @\, x=L \\ \hat{\mathcal{K}}_1\frac{\partial^2 w_1(0,t)}{\partial x^2} = -K_\theta\frac{\partial w_1(0,t)}{\partial x} \quad \text{and} \quad \frac{\partial^2 w_3(0,t)}{\partial x^2} = 0 \\ \hat{\mathcal{K}}_1\frac{\partial^3 w_1(0,t)}{\partial x^3} = -Kw_1(0,t) + F_{L1}(t) \qquad \hat{\mathcal{K}}_3\frac{\partial^3 w_3(0,t)}{\partial x^3} = -F_{L3}(t) \end{aligned} \quad , \quad (3)$$

where K_θ is the spring coefficient of an angular spring

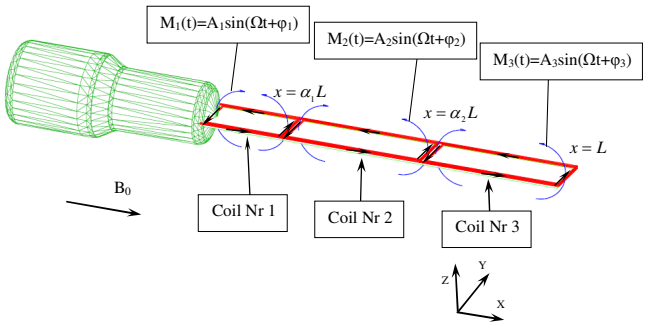

Fig. 2. Illustration of the swimming tail's operation. The interaction between the B_0 constant magnetic field of the MRI in the **x** direction and three alternating currents in three coils, (the direction of the current in each coil is designated by a black arrow) in the **y** direction creates alternating bending moments in the **z** direction. The moments have the same frequencies but different phases and amplitudes as shown.

located at the base of the beam, K is the coefficient of a linear spring located at the base of the beam. K_θ and K were added to the theoretical formulation in order to overcome the uncertainty of the clamping in the experimental setup and they are calibrated empirically. $F_{Li}(t) = N_i b_i I_i(t) B_0$ is the Lorenz force created by the magnetic field B_0. N_i is the number of turns in the i-th coil, b_i is the width of the coil, $I_i(t)$ is the current in the coil.

The continuity conditions at the boundaries between two coils are

$$@\ x = \alpha_1 L$$
$$w_1(\alpha_1 L, t) = w_2(\alpha_1 L, t)$$
$$\hat{\mathcal{K}}_1 \frac{\partial^2 w_1(\alpha_1 L, t)}{\partial x^2} = \hat{\mathcal{K}}_2 \frac{\partial^2 w_2(\alpha_1 L, t)}{\partial x^2}$$
$$\hat{\mathcal{K}}_1 \frac{\partial^3 w_1(\alpha_1 L, t)}{\partial x^3} + F_{L1}(t) = \hat{\mathcal{K}}_2 \frac{\partial^3 w_2(\alpha_1 L, t)}{\partial x^3} + F_{L2}(t)$$

and (4)

$$@\ x = \alpha_2 L$$
$$w_2(\alpha_2 L, t) = w_3(\alpha_2 L, t)$$
$$\frac{\partial w_2(\alpha_2 L, t)}{\partial x} = \frac{\partial w_3(\alpha_2 L, t)}{\partial x}$$
$$\hat{\mathcal{K}}_2 \frac{\partial^2 w_2(\alpha_2 L, t)}{\partial x^2} = \hat{\mathcal{K}}_3 \frac{\partial^2 w_3(\alpha_2 L, t)}{\partial x^2}$$
$$\hat{\mathcal{K}}_2 \frac{\partial^3 w_2(\alpha_2 L, t)}{\partial x^3} + F_{L2}(t) = \hat{\mathcal{K}}_3 \frac{\partial^3 w_3(\alpha_2 L, t)}{\partial x^3} + F_{L3}(t)$$

To solve the problem (2)-(4) by separation of variables method, one has to convert the boundary conditions. The conversion will result in a set of polynomials in the field equation and homogeneous boundary and continuity conditions.

The solution of the problem has the following form:

$$w_i(x,t) = \sum_{k=1}^{\infty} \phi_k^{(i)}(x) g_k(t) \ \forall i = 1,2,3 \quad (5)$$

In this solution (5), $\phi_k^{(i)}(x)$ is the shape of the *k*-th modal function in the segment *i*.

$g_k(t)$ is the tome function of the k-th mode of the beam.

$$g_k(s) = -\left(1 + \frac{s(s+2\zeta_k^{(1)}\omega_k)}{s^2 + 2\zeta_k^{(1)}\omega_k s + \omega_k^2} + \frac{s(s+2\zeta_k^{(2)}\omega_k)}{s^2 + 2\zeta_k^{(2)}\omega_k s + \omega_k^2} + \frac{s(s+2\zeta_k^{(3)}\omega_k)}{s^2 + 2\zeta_{3k}\omega_k s + \omega_k^2}\right)\sum_{i=1}^{3} Cp_k^{(i)} F_{Li}(s) \forall k = 1,2,...\infty \quad (6)$$

$\zeta_k^{(i)} \forall i = 1,2,3$ is the damping ratio in the i-th segment of the k-th mode, ω_k is the natural frequency of the k-th mode and $Cp_k^{(i)}$ is the decomposition of the polynomial that was used to convert the problem in the earlier steps of solution.

Since there are three inputs to the system $\mathbf{u} = [F_{L1}(s), F_{L2}(s), F_{L3}(s)]^T$, three-time function can be controlled $\mathbf{y} = [g_1(s), g_2(s), g_3(s)]^T$. We truncate (6) at the third mode and create a 3X3 square MIMO system, **y=P**(s)**u**. From the transfer matrix, **P**(s), we are able to find input **u** that gives the desired output, $\mathbf{y} = [g_1^{(d)}(s), g_2^{(d)}(s), g_3^{(d)}(s)]^T$ (see (1)) and activates the beam by open loop control. Further details on the calculation of the amplitudes $\{G_1, G_2, G_3\}$ and phases $\{\Phi_1, \Phi_2, \Phi_3\}$ see in [10].

Fig. 3 illustrates the motion created in the beam by the input forces calculated from the MIMO system based on (6).

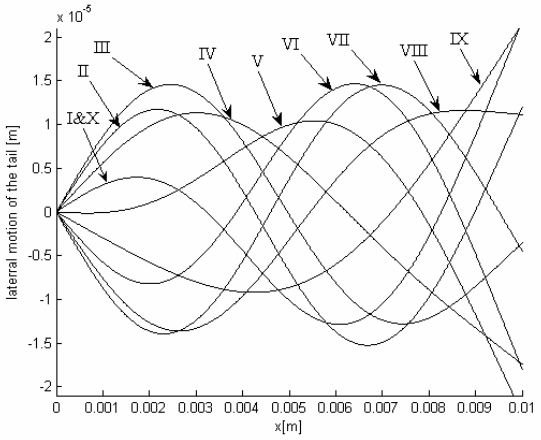

Fig. 3. Illustration of the motion of the tail by sequel snapshots of the tail simulation at ten different time-points (I~X).

D. Power generation in the MRI

Autonomous device to perform various functions require power to operate. Specifically the coils in the swimming tail require electric current to generate the waving motion of the tail. The required sinusoidal currents may be provided by either analog or digital circuitry which also requires additional power. The simplest way to power the circuits is to attach, enclose batteries with the autonomous device. Since this device relies on the static magnetic field (B_0) of the MRI, it is obvious to utilize the RF field (B_1) of the MRI to provide power to operate the tails. Coupling in power provides important advantages. One is that coils made of copper magnet wire are compatible with the MRI. Another advantage is that power can be provided any time by running

the scanner, unlike batteries, which may loose charge during the procedure.

The coupling of the power from the external transmit coil to the internal receive coil can be described by computing the magnetic field of the transmit coil at the location of the receive coil using the Biot-Savart Law.

$$B_1 = \mu_0 \frac{I}{2} \frac{a^2}{(a^2 + z^2)^{\frac{3}{2}}} \quad (7)$$

Where a is the radius of the circular coil z is the distance from the center of the coil on it's axis and I is the current in the coil. Since the field strength of the RF coils of an MRI is usually provided by the manufacturer, this step may be omitted.

The induced voltage is computed using Faraday's Induction Law, since the flux in the receiving coil and it's time derivative can be computed from the magnetic field. A coil having a surface area A and number of turns N, it's axis direction n_0 placed into a magnetic field of $B_1 sin(\omega t)$, the induced voltage V_i is:

$$V_i(t) = -\omega NA(B_0 \cdot n_0)\cos(\omega t) \quad (8)$$

When the direction of B_0 field is along the Z axis, the B_1 field is pretty much rotates in the X-Y plane of the Cartesian coordinate system of the MRI. The receiving coil may be facing any direction. To overcome the directional sensitivity of a single coil, we suggest to utilize a triplet of coils with their axes along the three axes of a Cartesian coordinate system. Using this setup results in an omni-directional receiver:

$$B_1 = \sqrt{(B_1 \cdot n_x)^2 + (B_1 \cdot n_y)^2 + (B_1 \cdot n_z)^2} \quad (9)$$

Where n_z, n_y, n_z are the directions of the coil triplet. Fig. 4. illustrates the omnidirectional coil triplet. The conversion

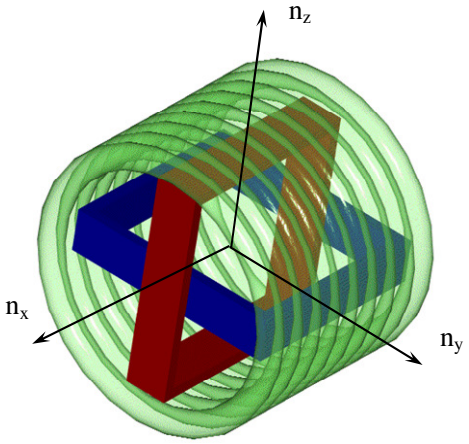

Fig. 4. Illustration of the receiving coil triplet with the coils normal axis. The outer cylindrical coil was made transparent for better illustration of the triplet.

from the power generator to the actuator will not be discussed in this paper.

Clinical MRI usually operates at high RF frequencies, thus the power receiving coil should be tuned to that frequency. With the correct tuning the voltage will increase by a factor of Q, where Q is the quality factor of the resonating circuitry. The load on the receiving coil may be simulated by a resistor attached to the coil's terminals. The resulting current flow will generate an opposing magnetic field, thereby reducing the voltage of the coil. The load also will lower the quality factor of the coil. Power matching happens, when the source resistance equals the load resistance. The resistance in a resonating circuitry may be computed by the formula of R = ωL/Q. Tuning and matching capacitors may be used to match the load resistance to the receiving coil.

III. Experimental Validation

A. Numerical Example

In order to estimate the feasibility of the suggested propulsive system, a single tail was designed and simulated by the analytical model. Considering the space limitations, the length of the swimming tail was chosen to be 10 mm, the width should be 5 mm and the total thickness should be 0.15 mm. The cross section of the tail depicts a copper wire coil mounted on a rectangular polymer film.

The coil is made of 100 turns (4 rows of 25 turns) of AWG 48 wire which dominates the stiffness of the tail. The three coils have lengths of: 4.3 mm, 3.7 mm and 2 mm in order from the cantilever base to the tip. The coils size are optimized to achieve the largest swimming velocity. The natural frequencies of the tail described above are: 294 Hz, 4.036 kHz and 12.836 kHz.

Calculation based on the theory presented above results in that we can produce a traveling wave of amplitude of 14 μm at 12.836 kHz (the third resonance frequency), assuming the current in the coils are 3.7 mA and the MRI's static magnetic field is 3T. The propulsive velocity of this tail is then 3 mm/s. The tail structure shown in Fig. 1 in which the tails are tilted by 30º to the axis of the capsule will achieve a maximal propulsive velocity of 7.9 mm/s. The force that is created in the tail is 5.5 mN.

To estimate the magnitude of the power available from a receiving coil, one was constructed out of AWG 32 copper magnet wire. A 5mm x 5mm rectangle coil, having 10 turns, had inductance of 1 μH and an unloaded quality factor of about 20. The self resonance of the coil was approximately 200MHz, which is above the Larmor frequency of the 3T MRI.

According Gandhi and Chen [12], at 128 MHz (3T) the magnetic field strength of a body coil is H = 6.52 A/m. Assuming vacuum's permeability to compute B_1, the induced voltage into the coil is $V_i = 1.64\,\mathrm{V}$. The voltage across the loaded terminals at optimally sized load is: $V_o = V_i Q/2 = 16.4\mathrm{V}$

The load resistance at optimum power matching should be 42 Ohms, therefore the current across it will be 0.2 A which is sufficient for powering our endoscopic capsule.

B. Validity study with a single coil

We conducted an experiment to assess the validity of theoretical and numerical design using copper magnet wire in 0.1T magnetic field.

An AWG 48 copper magnet wire was wound on a bobbin, to form a 4 mm by 10 mm rectangular coil. The width of 100 turns came to be about 1 mm. The wire bundle was impregnated with acetone. One of the 4 mm wide ends of the coil was attached to a plastic holder to create a cantilever of 8 mm length. Then the assembly was placed into a magnetic field strength of 0.1T. The coil was driven with a sinusoidal waveform from a signal generator via a 1 kOhm resistor. Fig. 5 shows the vibrating coil.

The voltage across the coil was monitored with an oscilloscope. Plotting the coil's current against it's voltage gave an indication of the resonance frequencies. Then around the first resonance frequency of the coil, point-by-point measurements were taken of both the amplitude and phase of the voltage of the coil. The signal generator output voltage provided the reference. Since the induced voltage is proportional to the movement of the coil, it was calculated from the measured values. The difference in the voltage across the coil when the coil is in and when it is out of the magnetic field yields the induced voltage, and the movement of the coil. The natural frequencies that were measured in the experiment were: 995 Hz, 18.1 kHz

The vibration of the swimming tail was compared to the analytical solution from in the previous chapter by setting the phase differences between the different coils to be zero. The theoretical natural frequencies were 996.2 [Hz], 18.2 [kHz] and 58.4 [kHz]. The spring coefficients were set to $\gamma_4 = \hat{\mathcal{K}} / K_\theta = 0.0385$ and $\gamma_5 = \hat{\mathcal{K}} / K = 0$ in order to fit the natural frequencies (ideally clamped boundary conditions are $\gamma_4 = \gamma_5 = 0$). The damping coefficient that was found was $\zeta = 0.012$ (equivalent to quality factor of Q=41.66). Fig. 6 shows the comparison of the experimental results (plus signs) to the theoretical ones (solid line). The data fits the theoretical results.

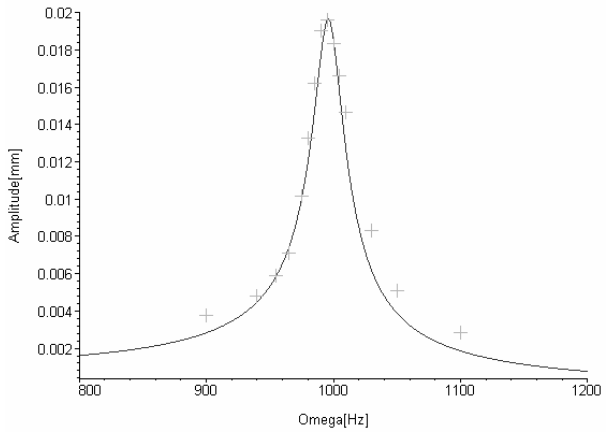

Fig. 6. Vibration of the around the first resonance (+ signs) compared with the theorethical prediction (solid line)

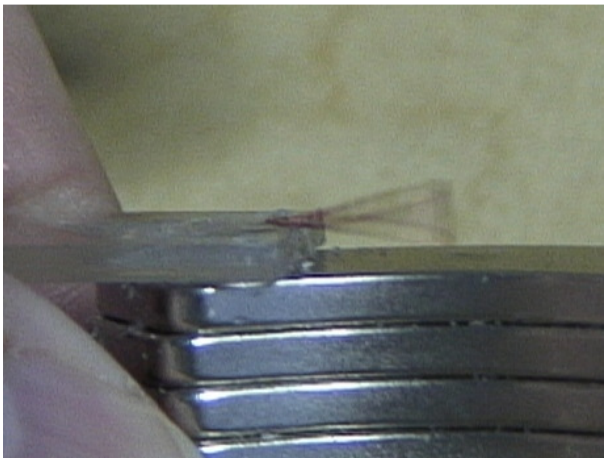

Fig. 5. Vibration of the cantilever at the first resonance driven by 160 mA at 1 kHz frequency.

To demonstrate power coupling into a single coil, a 9 cm diameter transmit coil was made from AWG 24 copper magnet wire. The resistance of the 250 turns was 7.2 Ohms. It was driven by the amplified signal of a waveform generator. The magnetic field generated 2 centimeters above the plane of the coil (driven by 5.4 A peak) was 14 mT peak.

The receiving coil was a single coil tail cantilever. This time a 10 Ohm resistor was placed over its terminals, to create current flow from the induced voltage. This first resonance frequency of the receiving coil was 1348 Hz. A 7.3 mV peak-peak voltage was recorded across the 10 Ohm resistor at resonance, equaling to a 0.365 mA peak current. Slightly off resonance, by ±20 Hz, the current in the coil was

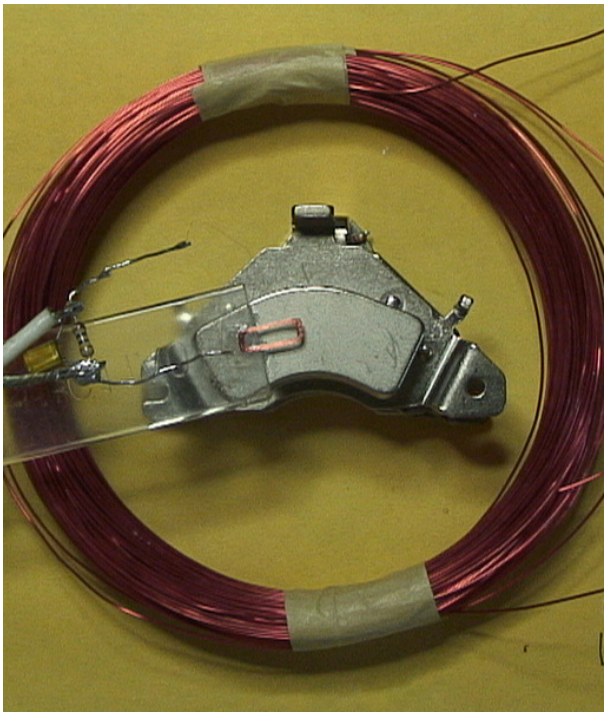

Fig. 7. The experimental setup that demonstrates the powering by induction..

0.66 mA, demonstrating that indeed the coil was vibrating significantly at its mechanical resonance.

IV. Conclusion

In this study, we presented, analytically and experimentally, a method to use capsule endoscopy within an MRI scanner. Traveling wave was induced into a swimming tail by electric currents and the B_0 of the MRI. The traveling wave can propel the capsule and controls it's location in the intestines. The currents in the tail coils can be powered by the B_1 field of the MRI. We found that a 10 mm long tail can propel the capsule with propulsive velocity of 7.9 mm/s and the magnetic bending force in the tail to be 5.5 mN and amount sufficient power is supplied. Vibration experiments showed that the model predicts accurately the resonance of the beam and may be used for the analysis of the swimming. This finding is consistent with those of a piezoelectric swimming tail [11]. Power supply experiment demonstrated the ability to create vibration by induction.

MRI, a minimally invasive yet very comprehensive imaging technology, is also adept at locating the capsule with respect to surrounding anatomical structures. However, the methods reported in the past used ferro-magnetic materials like permanent magnet in capsule and rotating magnetic fields to generate propulsion [3]. Such a propulsive mechanism cannot be combined with MRI due to the interaction of ferro-magnetic material with MRI's magnetic field. It is also difficult to place an additional set of magnetic field generators inside MRI or any other medical imager.

In contrast to legged capsules, our design is relatively simple and easy to fabricate [4],[5] and the actuators don't have to create large motion. The propulsive force is generated by multiple high frequency (12 kHz) sinusoidal signals having phase differences that create the traveling wave in the swimming tails. In addition, the high vibration frequency may prevent adhesion to the intestine walls.

The propulsion analysis in this study assumes that the propulsion is achieved through swimming not through proximity with the intestine walls. Preliminary theoretical investigations do show that swimming in the intestine is more efficient when in a confined space, it could be a factor, however.

In conclusion, we presented a new propulsion method that enables controlled capsule endoscopy in the MRI. In the near future a magnetic swimming tail will be built and tested in a full 3T MRI. At that time, we believe the novel technology will begin to realize it's full potential.

References

[1] G. Iddan, G. Meron, A. Glukhovsky, and P. Swain, "Wireless capsule endoscopy," *Nature*, vol. 405, pp. 417, May 2000.

[2] C. Ell, S. Remke, A. May, L. Helou, R. Henrich, and G. Mayer, "The first prospective controlled trial comparing wireless capsule endoscopy with push enteroscopy in chronic gastrointestinal bleeding,", *Endoscopy*, vol. 34, pp. 685-689, Sep. 2002.

[3] M. Sendoh, and K. Ishiyama, "Fabrication of Magnetic Actuator for Use in a Capsule Endoscope," *IEEE Transactions on Magnetics*, vol. 39, pp. 3232-3234, Sept. 2003.

[4] C. Stefanini, A. Menciassi, P. Dario, "Modeling and experiments on a legged microrobot locomoting in a tubular, compliant and slippery environment, *International Journal of Robotics Research*, vol. 25, pp. 551-560, May-June 2006.

[5] S. Gorini, M. Quirini, A. Menciassi, G. Pernorio, C. Stefanini, and P. Dario , "A Novel SMA Based Actuator for a Legged Endoscopic Capsule," in *Proc. first IEEE/RAS-EMBS International Conference on Biomedical Robotics and Biomechatronics*, Pisa, 2006, pp. 443-449.

[6] J. Happel and H. Brenner, *Low Reynolds number hydrodynamics*, Kluwer Boston, 1986, pp. 1-95.

[7] J.E. Colgate, and K.M. Lynch, "Mechanics and control of swimming: A review," *IEEE Journal of Oceanic Engineering* vol. 29, pp. 660-673, July 2004.

[8] G.I. Taylor, "The action of waving cylindrical tails in propelling microscopic organisms," *Proceedings of the Royal Society A*, vol. 211 pp. 225-239, Feb. 1952.

[9] G. Kósa, M. Shoham, and M. Zaaroor., "Propulsion of a Swimming Micro Medical Robot," in *Proc. 20th IEEE Conference on Robotics and Automation*, pp. 1339-1343, April 2005.

[10] G. Kósa, M. Shoham and M. Zaaroor., "Analysis of a Swimming Micro Medical Robot", in *Proc. first IEEE/RAS-EMBS International Conference on Biomedical Robotics and Biomechatronics*, Pisa, 2006, pp. 131-135.

[11] G. Kósa, M. Shoham and M. Zaaroor, "Propulsion Method for Swimming Micro Robots", *IEEE Transactions on Robotics*, vol. 23, pp. 137-150, Feb. 2007.

[12] O.P. Gandhi, and X.B. Chen, "Specific absorption rates and induced current densities for an anatomy-based model of the human for exposure to time-varying magnetic fields of MRI," Magnetic Resonance in Medicine, vol. 41, pp. 816-823, May 1999.